PROJECT ADMINISTRATION DATA SHEET

[x] ORIGINAL   [ ] REVISION NO. _____

Project No. __A-3063__   DATE __2/9/82__

Project Director: __T. G. Farrill__   School/Lab __RAIL/RDD__

Sponsor: __Vought Corporation, Dallas, TX__

Type Agreement: __Purchase Order No. P-322228 (Prime DASG60-81-C-0083)__

Award Period: From __9/1/81__ To __1/31/82__ (Performance) _____ (Reports)

Sponsor Amount: __$28,587__   Contracted through:

Cost Sharing: __None__   GT.../GTT

Title: __Small Radar Homing Interceptor Technology (SRHIT) Sensor Study Support__

ADMINISTRATIVE DATA

OCA Contact __William F. Brown__

1) Sponsor Technical Contact:

2) Sponsor Admin/Contractual Matters:

Mr. B. R. Henry, Subcontract Adm.

M/S 49-78, Dept. 2-88100

Vought Corp.

P. O. Box 22614

Dallas, TX 75266

(214) 266-2279

Defense Priority Rating: __DX-A2__   Security Classification: __None__

RESTRICTIONS

See Attached __None__ Supplemental Information Sheet for Additional Requirements.

Travel: Foreign travel must have prior approval — Contact OCA in each case. Domestic travel requires sponsor approval where total will exceed greater of $500 or 125% of approved proposal budget category.

Equipment: Title vests with __None proposed or anticipated__

COMMENTS:

Effort completed in January 1982. EES Accounting - please bill sponsor.

COPIES TO:

Administrative Coordinator	Research Security Services	EES Public Relations (2)
Research Property Management	Reports Coordinator (OCA)	Computer Input
Accounting	Legal Services (OCA)	Project File
Procurement/EES Supply Services	Library	Other _____

FORM OCA 4:781

GEORGIA INSTITUTE OF TECHNOLOGY   **OFFICE OF CONTRACT ADMINISTRATION**

SPONSORED PROJECT TERMINATION SHEET

Date ___5/12/82_____

Project Title: Small Radar Homing Interceptor Technology (SRHIT) Sensor Study Support

Project No: A-3063

Project Director: T. G. ~~Farrill~~/Farill

Sponsor: Vought Corporation, Dallas, TX

Effective Termination Date: ___1/31/82_____

Clearance of Accounting Charges: ___1/31/82_____

Grant/Contract Closeout Actions Remaining:

[x] Final Invoice and Closing Documents

[ ] Final Fiscal Report

[x] Final Report of Inventions

[x] Govt. Property Inventory & Related Certificate

[ ] Classified Material Certificate

[ ] Other _____

Assigned to: ___RAIL/RDD_____ (School/Laboratory)

COPIES TO:

Administrative Coordinator	Research Security Services	EES Public Relations (2)
Research Property Management	Reports Coordinator (OCA) ✓	Computer Input
Accounting	Legal Services (OCA)	Project File
Procurement/EES Supply Services	Library	Other _____

ENGINEERING EXPERIMENT STATION

Georgia Institute of Technology
A Unit of the University System of Georgia
Atlanta, Georgia 30332

16 February 1982

Vought Corporation
P. O. Box 26114
Dallas, TX 75266

Attention: Mr. B. R. Henry

Subject: Purchase Order P-322228

Dear Mr. Henry:

Attached is draft material documenting analyses performed at Georgia Tech in response to your SOW and verbal requests of Paul Cunningham. The material is for use in your final report as appropriate.

This submittal completes all effort to be performed under the subject purchase order.

Very truly yours,

Trent G. Farill
Project Director

TGF/vcy

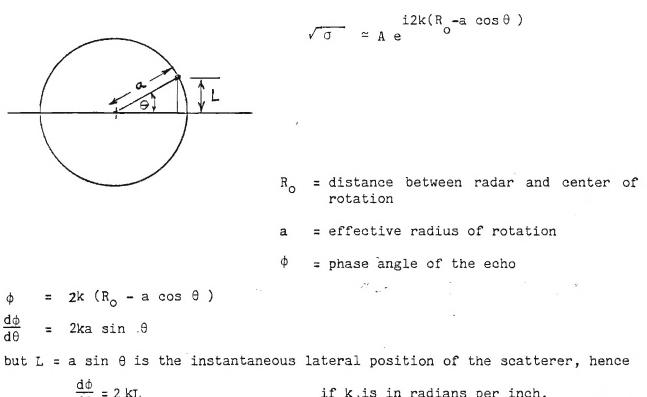# RADAR CROSS SECTION AND GLINT CALCULATION

INTRODUCTION

For the purpose of estimating the glint characteristics of a simple target, one needs to know the rate of change of phase of the return signal with respect to the aspect angle. Fortunately a computer program was available [1] for bodies of roll symmetry and perfectly conducting surfaces. The computer program is based on the physical optics prescription for the scattering from surface elements and on the geometrical theory of diffraction for edges. The latter implicitly contains polarization dependence while the former does not. Thus, glint characteristics can be predicted for arbitrary polarizations. However, for simplicity, the data given below are for the principal polarizations only.
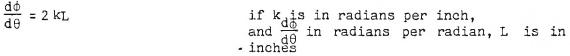
The program is a coherent one, in that the phase angles of the contributions from various portions of the target are "remembered." The phase angle of the sum of the contributions can be output (as shown below), and can also be used to form the rate of change. The basic program described in [1] was slightly modified to do this. The results are typical of what the program can do, and other bodies of revolution can easily be simulated.

---

[1]   E. F. Knott and T. B. A. Senton, "A Program Incorporating Diffraction for the Computation of Radar Cross Section," University of Michigan, Report 011758-2-T, June 1973.

Point Scatterer

$$\sqrt{\sigma} \simeq A\, e^{\,i2k(R_o - a\cos\theta)}$$

R_o = distance between radar and center of rotation

a = effective radius of rotation

ϕ = phase angle of the echo

$\phi = 2k\,(R_o - a\cos\theta)$

$\dfrac{d\phi}{d\theta} = 2ka\sin\theta$

but $L = a\sin\theta$ is the instantaneous lateral position of the scatterer, hence

$$\frac{d\phi}{d\theta} = 2\,kL$$

if k is in radians per inch, and $\dfrac{d\phi}{d\theta}$ in radians per radian, L is in inches

$$\therefore\ L = \frac{1}{2k}\frac{d\phi}{d\theta}$$

Thus, apparent glint is large where the rate of change of phase with aspect angle is large.

ANALYSIS

The program returns amplitude and phase of the backscattering for horizontal and vertical polarizations. The amplitude data are expressed in dB above a square wavelength. The return from the spherical nose of the RV is given by the formulat for a sphere:

$$\frac{\sigma}{\lambda 2} = \pi\ \left(\frac{a}{\lambda}\right)^2$$

The radius of the sphere is 3.15 inches, and its radar cross section is -17.0 dBm². Normalized with respect to the square of the wavelength, we get

$$\frac{\sigma}{\lambda^2} = \begin{array}{lll} 18.4\text{ dB} & (17.5\text{ GHz}) & \\[4pt] & & \text{nose returns} \\[4pt] 24.4\text{ dB} & (35\text{ GHz}) & \end{array}$$

The return from the base of the cone at axial incidence is independent of the frequency (2),

$$\sigma = 4\pi \; \frac{r \, \sin\,(\pi/n)}{n\,(\cos\dfrac{\pi}{n} - \cos\dfrac{3\pi}{n})}$$

where r is the radius of the base and n is the normalized exterior wedge angle of the base,

$$n = 1.5 + \frac{\alpha}{\pi}$$

where α is the cone half-angle (7° in our case). For a base radious of 11.811 inches, we calculate the base return to be

$$\frac{\sigma}{\lambda^2} = \quad \begin{matrix} 28.0 \text{ dB} & (17.5 \text{ GHz}) \\[4pt] 34.0 \text{ dB} & (35 \text{ GHz}) \end{matrix} \qquad \text{base returns}$$

Thus the nose return is about 9.6 dB below the base return at both frequencies.

Depending on the relative phase of the nose and base returns, the net echo could range from 3.4 dB below the base return to 2.5 dB above it. Thus the on-axis amplitude should be somewhere between 24.6 and 30.5 dB above a square wavelength at 17.5 Ghz, and between 30.6 and 36.5 at 35 GHz.
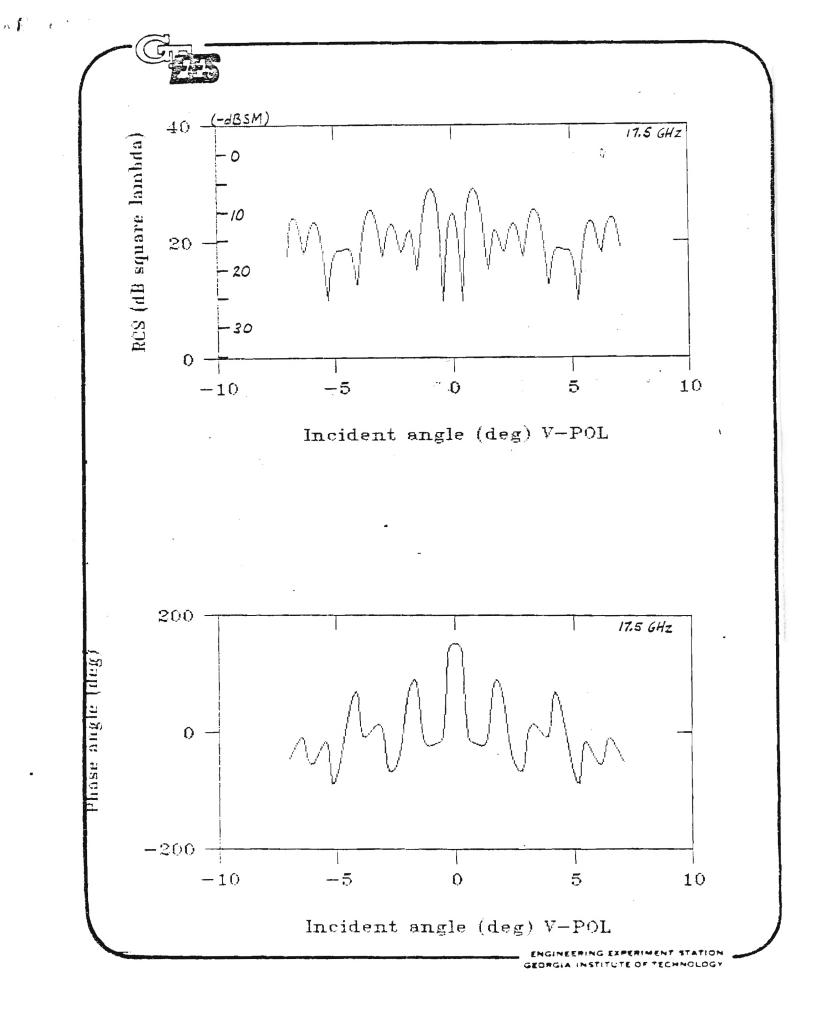
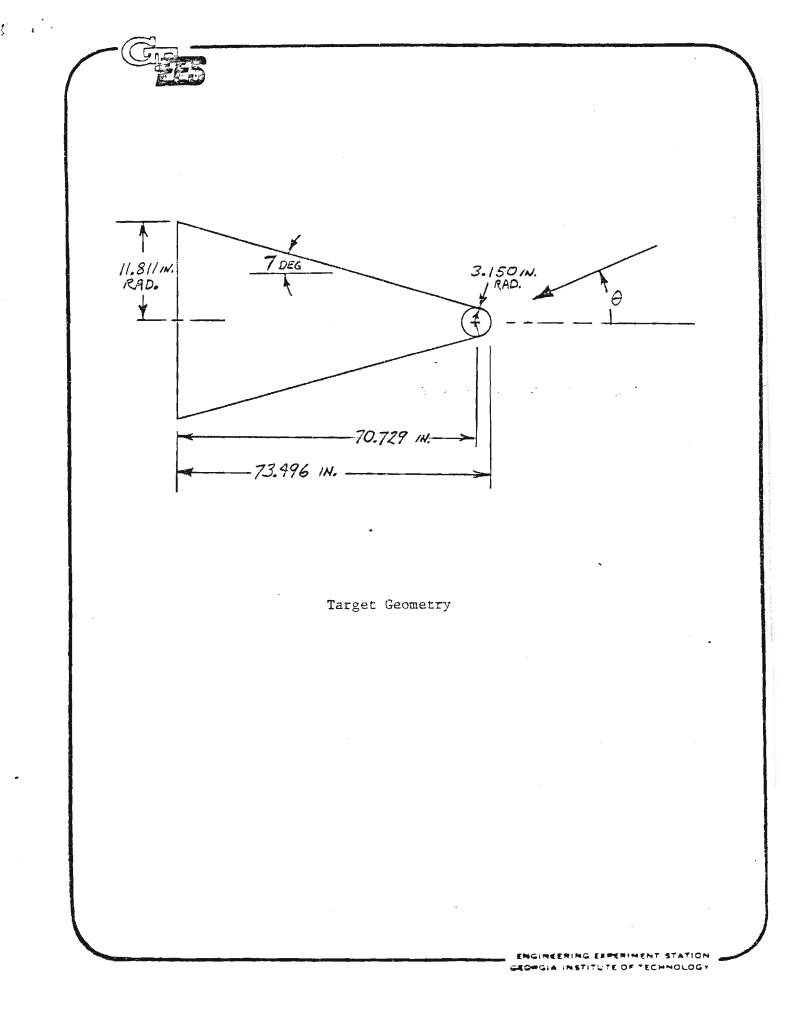The table below summarizes the nose-on amplitudes:

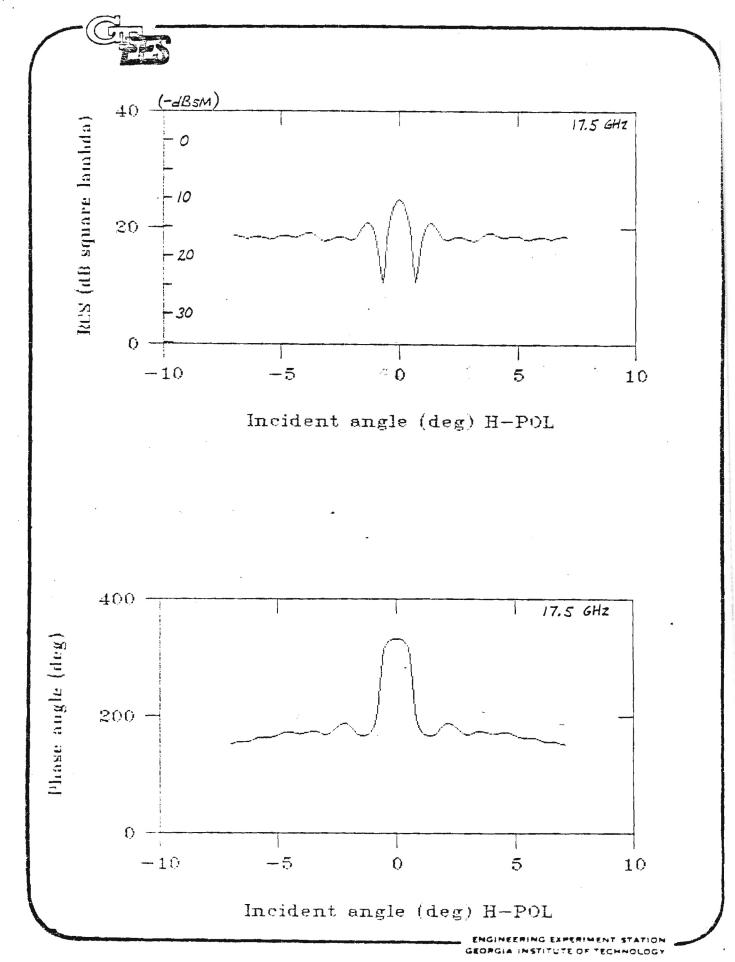| f, GHz	σ, dBλ^2 from above analysis	σ, dBλ^2 from plots
17.5	24.6 - 30.5	24.9
35.0	30.6 - 36.5	31.4

Thus, the predicted patterns seem correct.

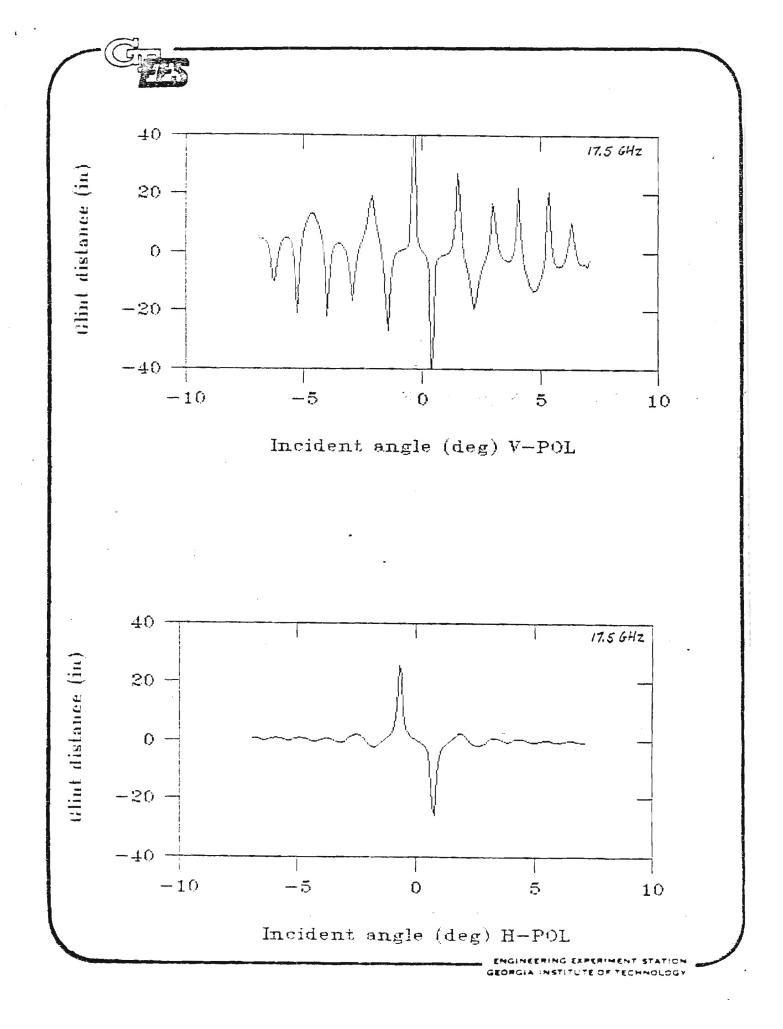[2] J. B. Keller, "Backscattering from a Finite Cone," IRE Transactions on Antennas and Propagation, Vol. AP-8, March 1960, pp. 175-182.
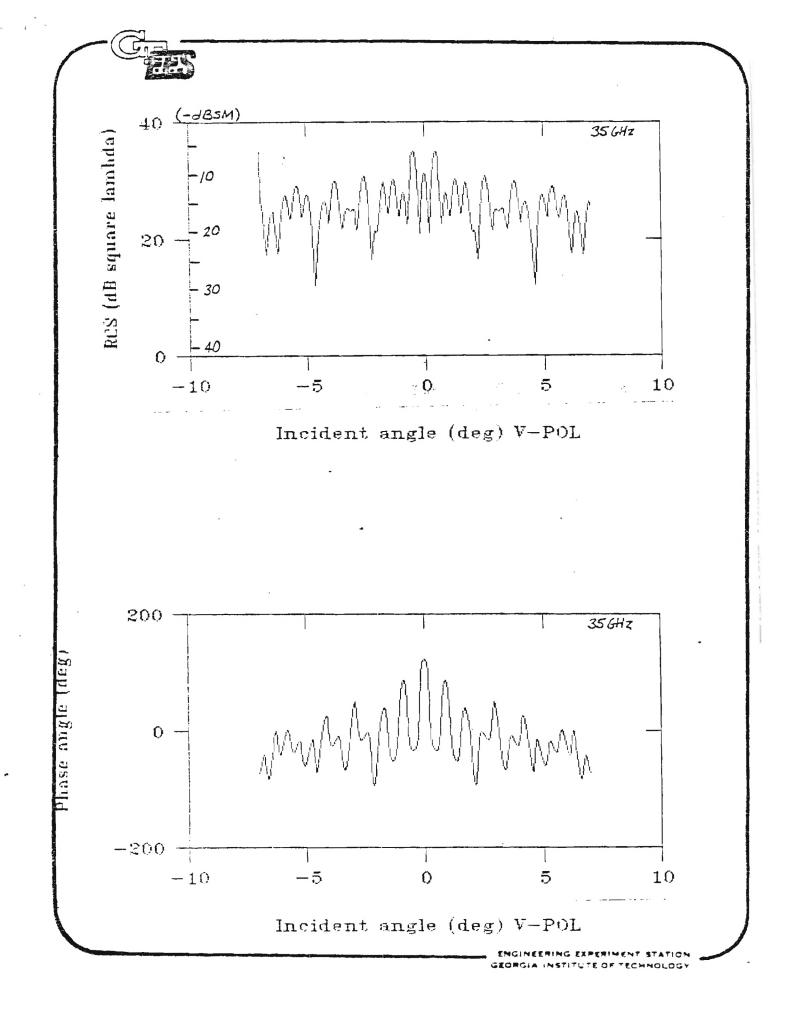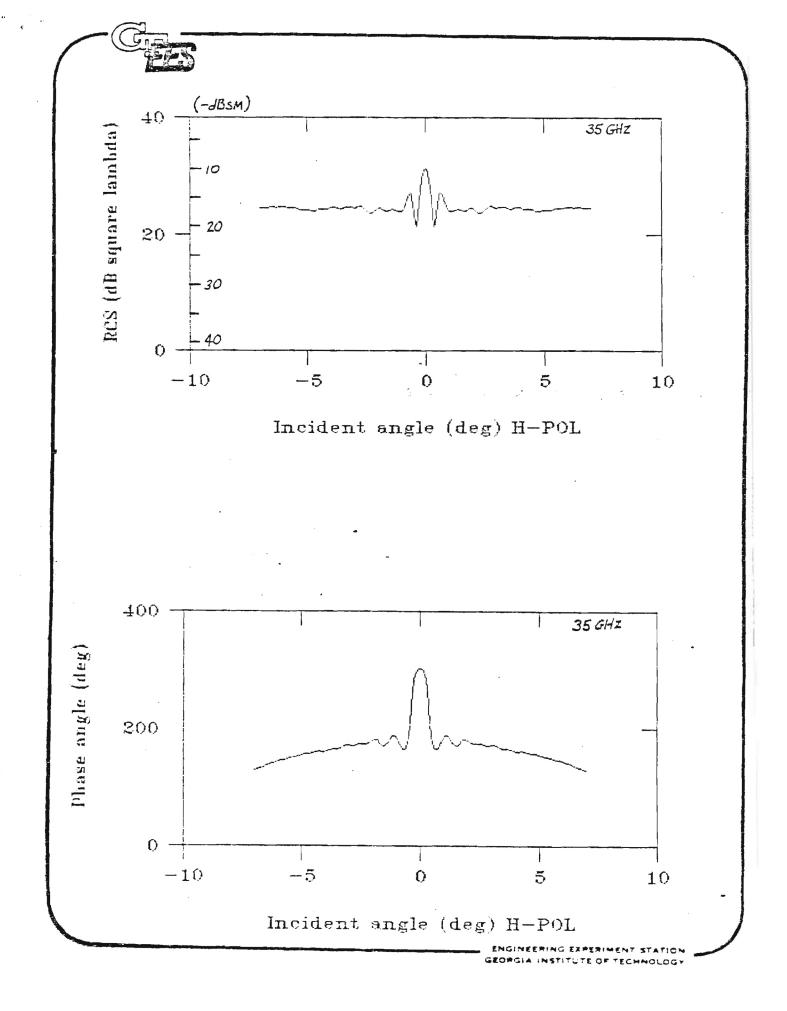
Incident angle (deg) V-POL

Incident angle (deg) V-POL

11.811 IN. RAD.

7 DEG

3.150 IN. RAD.

θ

70.729 IN.

73.496 IN.

Target Geometry

Incident angle (deg) H-POL

Incident angle (deg) H-POL

Glint distance (in) vs. Incident angle (deg) V-POL — 17.5 GHz

Glint distance (in) vs. Incident angle (deg) H-POL — 17.5 GHz

Incident angle (deg) V-POL

Incident angle (deg) V-POL

Incident angle (deg) H-POL

Incident angle (deg) H-POL
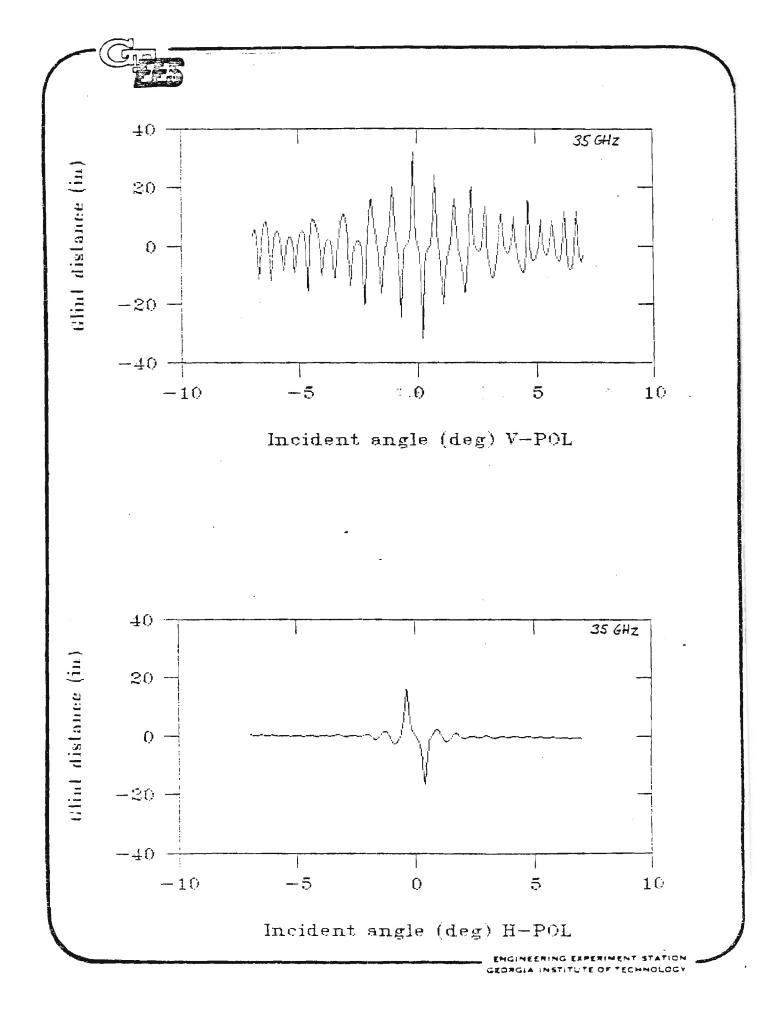
Incident angle (deg) V–POL

Incident angle (deg) H–POL
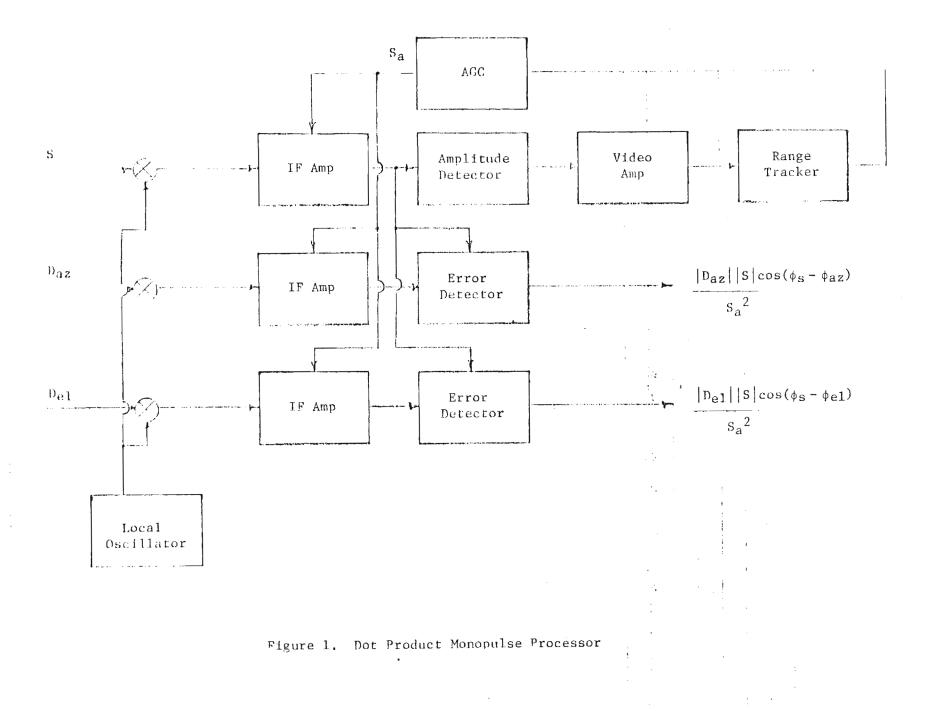
MONOPULSE ANGLE MEASUREMENT ERROR

This section is concerned with the mean and standard deviation of angle errors in monopulse systems caused by thermal noise. Two representative monopulse implementations are analyzed: the dot product processor with long time constant AGC and the phase comparison or $S \pm jD$ processor. Single pulse errors are derived and extended to multiple pulse cases for coherent and noncoherent integration. The mathematical expressions for the mean and standard deviation of the error are valid for arbitrary signal to noise ratio (ρ) and can be simplified for limiting value of ρ.

1. SINGLE PULSE

Single pulse thermal noise measurement errors for the monopulse systems shown in Figures 1 and 2 are derived in terms of the antenna parameters and the input signal to noise ratio. The operation and advantage/disadvantage of each implementation are also discussed.
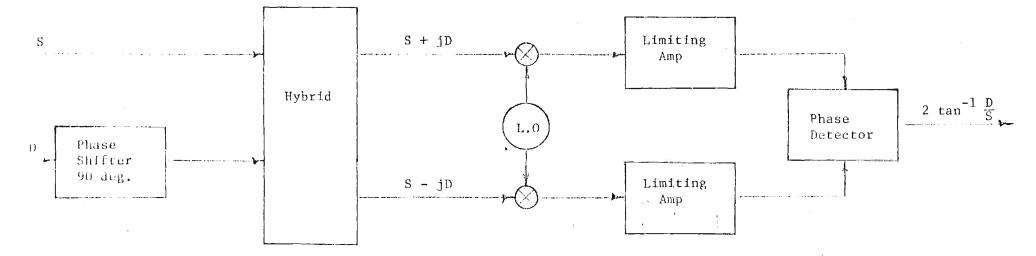
1.1 Dot Product Detector

The commonly used dot product processor (Figure 1) has 3 receiver channels: one each for the sum signal and the two difference signals. A long time constant AGC circuit (averaging over many pulses) normalizes the IF signals to the sum signal. The normalized sum signal is used for display and range tracking purposes; it is also input to the error detectors along with the normalized difference signals to generate the monopulse or error characteristic. In the absence of noise the outputs of the error detectors are equal to the ratio of D to S and proportional to the angle of the target from boresight. System noise generated primarily by the mixers causes bias and random errors in the angle measurement process. The main disadvantage of the dot product processor is degradation in performance when the target

Figure 1. Dot Product Monopulse Processor

S

$S + jD$

Limiting
Amp

O

Phase
Shifter
90 deg.

Hybrid

L.O

$2 \tan^{-1} \dfrac{D}{S}$

Phase
Detector

$S - jD$

Limiting
Amp

Figure 2.   S ± jD Monopulse Processor

RCS fluctuates on a pulse to pulse basis; in this case the AGC output averaged over several pulses is not equal to the sum signal of an individual pulse and significant errors are introduced in the normalization process.

At the outputs of the IF amplifiers the sum and difference signals during the reception of the target pulse can be written in the form:

$$[A_O |S(\theta)| \cos(\omega t + \phi_s)$$
$$+ x_1(t) \cos \omega t - y_1(t) \sin \omega t] \frac{1}{\sqrt{P}} = s(t) \qquad (1a)$$

$$[A_O |D(\theta)| \cos(\omega t + \phi_d)$$
$$+ x_2(t) \cos \omega t - y_2(t) \sin \omega t] \frac{1}{\sqrt{P}} = d(t) \qquad (1b)$$

where $|S(\theta)|$ is the magnitude of the antenna sum voltage pattern, $|D(\theta)|$ is the magnitude of the antenna difference voltage pattern, ϕ_s is the phase in the sum channel, ϕ_d is the phase in the difference channel, A_0 is an amplitude proportional to the square root of the received power, $x_1(t)$ and $y_1(t)$ are the quadrature Gaussian noise components in the sum channel having zero means and variances equal to the noise power, $x_2(t)$ and $y_2(t)$ are the quadrature Gaussian noise components in the difference channel and $\sqrt{P}$ is the normalized amplitude of the AGC output. For a long time constant AGC circuit, P is approximately equal to the sum of the signal and noise powers in the sum channel averaged over several successive pulses. If the signal and noise powers are constant over the response time of the AGC circuit, then

$$P = P_s + P_n$$

where P_S and P_n are the single pulse signal and noise powers in the sum channel. The AGC normalizing amplitude in this case is then

$$\sqrt{P} = \sqrt{P_S + P_n} \tag{2}$$

The error detector can be modeled as a mixer followed by a low pass filter. Thus the output voltage of an error detector with inputs equal to those given by Equations (1a) and (1b) is:

$$
\begin{aligned}
f(t) = \frac{1}{2P} \{ & A_0{}^2 \, |D(\theta)| \, |S(\theta)| \, \cos(\phi_S - \phi_d) \\
& + A_0 \, |S(\theta)| \, [x_2(t) \, \cos\phi_S + y_2(t) \, \sin\phi_S] \\
& + A_0 \, |D(\theta)| \, [x_1(t) \, \cos\phi_d + y_1(t) \, \sin\phi_d] \\
& x_1(t) \, x_2(t) + y_1(t) \, y_2(t) \}
\end{aligned}
\tag{3}
$$

For zero noise and constant receive signal power, the output is

$$
\begin{aligned}
f_0(t) &= \frac{A_0{}^2 \, |D(\theta)| \, |S(\theta)| \, \cos(\phi_S - \phi_d)}{2P_S} \\
&= \frac{|D(\theta)|}{|S(\theta)|} \, \cos(\phi_S - \phi_d) = \frac{D(\theta)}{S(\theta)} \, .
\end{aligned}
\tag{4}
$$

where

$$P_S = \frac{A_0{}^2 \, |S(\theta)|^2}{2} \, . \tag{5}$$

Over a region of plus or minus 1/2 beamwidth about the antenna

axis the monopulse characteristic is approximately linear:

$$\frac{|D(\theta)|}{|S(\theta)|} \cos(\phi_s - \phi_d) \cong \frac{k_m \theta_t}{\Delta \theta} = k\theta_t \qquad (6)$$

where θ_t is the target angle with respect to axis, $\Delta \theta$ is the sum pattern 3 dB beamwidth and k_m is a constant approximately equal to 1.57. Hence the angle estimate in the noise free case is

$$\hat{\theta} = \frac{f_o(t)}{k} \qquad (7a)$$

and in the noisy case

$$\hat{\theta} = \frac{f(t)}{k} \quad . \qquad (7b)$$

The error in the angle estimate is then

$$\epsilon = \hat{\theta} - \theta_t = \frac{f(t)}{k} - \theta_t \quad . \qquad (8)$$

Quality of the estimate is usually determined by the mean and standard deviation of the estimate error. The expected value of the error is

$$E(\epsilon) = \frac{E(f)}{k} - \theta_t . \qquad (9)$$

In Equation (3) for $f(t)$ the random variables x_1, x_2, y_1, y_2 are independent Gaussian random variables with zero means. Therefore only the first term contributes to the mean:

$$\frac{E(f)}{k} = \frac{A_o^2 |D(\theta)| \ |S(\theta)| \ \cos(\phi_s - \phi_d)}{2Pk} \quad . \qquad (10)$$

Substituting Equation (6) in the numerator and Equation (2) in the denominator of Equation (10) it is found that

$$\frac{E(f)}{k} = \frac{A_o^2 |S(\theta)|^2 \theta_t}{2(P_s + P_n)} \qquad (11)$$

which reduces to

$$\frac{E(f)}{k} = \frac{P_s \theta_t}{P_s + P_n}$$

when Equation (5) is used for P_s. The mean error is then

$$E(\epsilon) = \theta_t \left(\frac{P_s}{P_s + P_n} - 1 \right) = - \frac{\theta_t}{1 + \rho} \tag{12}$$

where ρ is the single pulse signal to noise ratio. Equation (12) indicates that the AGC operation which produces a normalizing factor proportional to the sum of the signal and noise powers in the sum channel introduces a bias error proportional to the angle of the target from boresight. Only for large values of ρ is the bias error insignificant.

The variance of the error is

$$
\begin{aligned}
Var(\epsilon) &= E \left[\epsilon - E(\epsilon) \right]^2 \\
&= E \left\{ A_o \left| S(\theta) \right| \left[x_2 \cos \phi_s + y_2 \sin \phi_s \right] \right. \\
&\quad + A_o \left| D(\theta) \right| \left[x_1 \cos \phi_d + y_1 \sin \phi_d \right] \\
&\quad \left. + x_1 x_2 + y_1 y_2 \right\}^2 / 4P^2 k^2
\end{aligned}
\tag{13}
$$

Since x_1, y_1, x_2, y_2 are mutually independent with zero means and variances $E(x_1{}^2) = E(y_1{}^2) = \sigma_1{}^2$, $E(x_2{}^2) = E(y_2{}^2) = \sigma_2{}^2$ where $\sigma_1{}^2$ and $\sigma_2{}^2$ are the noise powers in the sum and difference channels, respectively, the error variance becomes

$$Var(\epsilon) = \frac{A_o{}^2 \left| S(\theta) \right|^2 \sigma_2{}^2 + A_o{}^2 \left| D(\theta) \right|^2 \sigma_1{}^2 + 2\sigma_1{}^2 \sigma_2{}^2}{4P^2 k^2} \tag{14}$$

Assuming equal noise powers in the two channel and substituting the expression for A_O as given by Equation (5) into Equation (14), the variance reduces to

$$Var(\varepsilon) = \frac{2P_s\,P_n + 2P_s\,P_n\,\left|\frac{D(\theta)}{S(\theta)}\right|^2 + 2P_n^2}{4k^2\,(P_s + P_n)^2} \tag{15}$$

Taking the square root of Equation (15) and substituting for k from Equation (6) the standard deviation of the error becomes

$$\sigma_\varepsilon = S.D.(\varepsilon) = \frac{\Delta\theta}{k_m}\left[\frac{P_s\,P_n\left(1 + \left|\frac{D(\theta)}{S(\theta)}\right|^2\right) + P_n^2}{2\left(P_s + P_n\right)^2}\right]^{1/2} \tag{16}$$

In terms of the single pulse signal to noise rate ρ,

$$\sigma_\varepsilon = \frac{\Delta\theta}{k_m}\left[\frac{1 + \left|\frac{D(\theta)}{S(\theta)}\right|^2 + \frac{1}{\rho}}{2\rho\left(1 + \frac{1}{\rho}\right)^2}\right]^{1/2} \tag{17}$$

If the target is close to the boresight so that $\left|\frac{D(\theta)}{S(\theta)}\right| \ll 1/\rho$ then

$$\sigma_\varepsilon \cong \frac{\Delta\theta}{k_m\,\sqrt{2\,(\rho + 1)}} \tag{18}$$

Note that only when $\rho \gg 1$ and $|D(\theta)/S(\theta)| \ll 1$ does the standard deviation of the error reduce to the commonly quoted relationship

$$\sigma_\varepsilon = \frac{\Delta\theta}{k_m\sqrt{2\rho}} \ .$$

In the general case, Equation (16) should be used to evaluate σ_ε.

1.2   S ± jD Processor

Figure 2 shows a block diagram of the S ± jD or phase monopulse processor. The difference signal is shifted by 90 degrees and combined with the sum signal in a hybrid to produce phase modulated signals at RF. Conversion to IF is accomplished by using mixers and a common local oscillator (L.O.). The signals in each channel are hard limited in the limiting amplifiers to normalize the signals and eliminate any amplitude modulation. Synchronous detection in a phase detector produces an output voltage which is proportional to the phase difference between the signals in the two channels. The phase difference is proportional to the ratio of D to S and is converted to target angle with respect to boresight by dividing by the known monopulse slope. Phase processing normalizes the signals on a pulse to pulse basis and eliminates the problems of amplitude fluctuation associated with the AGC of the dot product processor.

At the output of the mixers the signals in the two channels can be written as

$$f_1(t) = R_e \left\{ \left[A |S(\theta)| e^{j\phi_S} + jA |D(\theta)| e^{j\phi_d} \right. \right.$$
$$\left. \left. + x_1(t) + j\, y_1(t) \right] e^{j\omega_o t} \right\}$$
$$= R_e \left(A_1\, e^{j\phi_1}\, e^{j\omega_o t} \right). \tag{19a}$$

$$f_2(t) = R_e \left\{ \left[A|S(\theta)|\, e^{j\phi_S} - jA|D(\theta)|\, e^{j\phi_d} \right. \right.$$
$$\left. \left. + x_2(t) + jy_2(t) \right] e^{j\omega_o t} \right\}$$
$$= R_e \left(A_2\, e^{j\phi_2}\, e^{j\omega_o t} \right) , \tag{19b}$$

where $|S(\theta)|$, ϕ_S and $|D(\theta)|$, ϕ_d are the amplitude and phase of the antenna one way voltage sum and difference patterns, respectively; $x_1(t), y_1(t)$ and $x_2(t), y_2(t)$ are the quadrature Gaussian noise components with zero means and variances equal to the noise power introduced by the mixers in each IF channel; A is an amplitude related to the received sum signal power P_S through the equation

$$P_S = A^2 |S(\theta)|^2 \tag{20}$$

A_1, ϕ_1 and A_2, ϕ_2 are the envelopes and phases in the repsective channels. If no phase errors are introduced in the system, then for target angles within ± 1/2 beamwidth of boresight $\phi_S = 0$ and $\phi_d = 0$ or 180 degrees. Thus $|S(\theta)| e^{j\phi_S}$ and $|D(\theta)| e^{j\phi_d}$ can be written as the real quantities $S(\theta)$ and $D(\theta)$ where $S(\theta)$ is always positive and $D(\theta)$ is bipolar.

In the absence of noise the output of the phase detector is a function of the phase difference between the signals in the two channels,

$$u = f(\Delta\phi) = f(\phi_1 - \phi_2) = f\left(2 \tan^{-1} \frac{D}{S}\right) \tag{21}$$

where the phase detector function has the sawtooth shape shown in Figure 3. Within $\pm 1/2$ beamwidth of boresight:

$$\frac{D(\theta)}{S(\theta)} = k\ \theta_t$$

and

$$\Delta\phi = 2 \tan^{-1} k\ \theta_t.$$

For small target angles

$$\tan^{-1} k\theta_t \cong k\theta_t$$

and the estimated target angle $\hat{\theta}$ is related to the phase detector output as

$$\hat{\theta} = \frac{f(\Delta\phi)}{2k} = \frac{u}{2k}. \tag{22}$$

When the thermal noise contributed by the mixers is included, the estimate becomes

$$\hat{\theta} = \frac{f(\phi_1 - \phi_2)}{2k} = \frac{f(\Delta\phi)}{2k}$$

$$= \frac{1}{2k}\ f\left[\tan^{-1} \frac{A\ D(\theta) + y_1(t)}{A\ S(\theta) + x_1(t)} - \tan^{-1} \frac{-A\ D(\theta) + y_2(t)}{A\ S(\theta) + x_2(t)}\right] \tag{23}$$
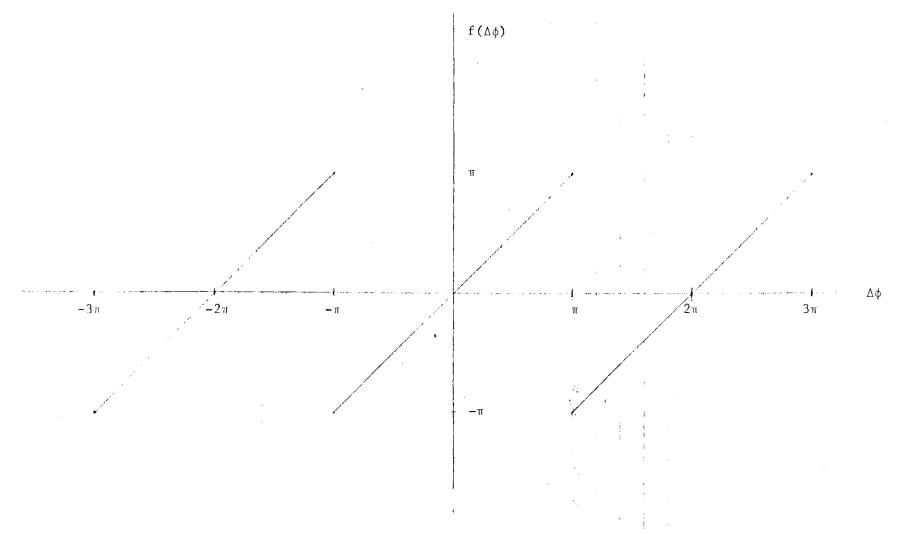
Figure 3. Phase Detector Functional Relationship.

In order to calculate the mean and standard deviation of the error, the probability density of $\phi_1 - \phi_2 = \Delta\phi$ must be derived and transformed to the density for $f(\Delta\phi)$. Now ϕ_1 and ϕ_2 are independent random variables because ϕ_1 is a function of x_1 and y_1, ϕ_2 is a function of x_2 and y_2 and x_1, y_1, x_2, y_2 are mutually independent. Thus the density of $\Delta\phi$ is determined by deriving the individual densities for ϕ_1 and $-\phi_2$ and forming their convolution.

From Equation (23) it is seen that ϕ_1 is the arctangent of the ratio of two independent Gaussian random variables. The numerator, $y = A\,D(\theta) + y_1$, has a mean of $A\,D(\theta)$ and a variance of σ_1^2 equal to the noise power P_{n1} in the S + jD channel; the denominator, $x = A\,S(\theta) + x_1$ has a mean $A\,S(\theta)$ and a variance σ_1^2. Since x_1 and y_1 are independent, the joint probability of x and y is

$$p(x,y) = p(x)\,p(y)$$
$$= \frac{1}{2\pi\,\sigma_1^2}\,\exp\left[-\frac{(x - A\,S)^2}{2\,\sigma_1^2} - \frac{(y - A\,D)^2}{2\,\sigma_1^2}\right]. \tag{24}$$

Changing variables to r and ϕ_1 where

$$x = r\cos\phi_1 \qquad\qquad r = \sqrt{x^2 + y^2}$$

$$y = r\sin\phi_1 \qquad\qquad \phi_1 = \tan^{-1} y/x$$

the joint probability of r and ϕ_1 becomes

$$p(r,\phi_1) = \frac{r}{2\pi\,\sigma_1^2}$$
$$\exp\left[\frac{-r^2 + 2r\,AB\cos(\phi_1 - \psi) - A^2 S^2 - A^2 D^2}{2\sigma_1^2}\right] \tag{25}$$

with $B = \sqrt{D^2 + S^2}$ (26a)

$\psi = \tan^{-1} D/S.$ (26b)

The density for ϕ_1 is obtained by integrating Equation (25) with respect to r from zero to infinity. Using the identities:

$$\exp[Z \cos\gamma] = I_0(Z) + 2 \sum_{n=1}^{\infty} I_n(Z) \cos n\gamma \qquad (27a)$$

$$I_n(Z) = (-j)^n J_n(jZ) \qquad (27b)$$

the density for ϕ_1 becomes

$$p(\phi_1) = \int_0^{\infty} \frac{r}{2\pi \sigma_1^2}$$

$$\left[J_0\left(\frac{jrAB}{\sigma_1^2} \right) + 2 \sum_{n=1}^{\infty} (-j)^n J_n\left(\frac{jrAB}{\sigma_1^2} \right) \cos(n\phi_1 - n\psi) \right]$$

$$\exp\left[\frac{-A^2 S^2 - A^2 D^2 - r^2}{2\sigma_1^2} \right] dr \qquad (28)$$

where J_n is the Bessel function of the first kind of order n and I_n is the modified Bessel of the first kind of order n. Reference 1 lists the following integral identities:

$$\int_0^{\infty} e^{-a^2 t^2} t^{n+1} J_n(bt) \, dt = \frac{b^n}{(2a^2)^{n+1}} e^{-\frac{b^2}{4a^2}} \qquad (29a)$$

$$\int_0^\infty e^{-a^2 t^2} t^{k-1} J_n(bt) \, dt$$

$$= \frac{\Gamma\left(\frac{n+k}{2}\right) \left(\frac{b}{2a}\right)^n}{2a^k \, \Gamma(n+1)} M\left(\frac{n+k}{2}, \, n+1; \, -\frac{b^2}{4a^2}\right) \tag{29b}$$

where Γ denotes the gamma function and M is the confluent hyper-geometric or Kummer's function. For

$$t = r$$
$$a^2 = \frac{1}{2\sigma_1^2}$$

$$b = \frac{jAB}{2\sigma_1^2}$$

with $n = 0$ in Equation (29a) and $k = 2$ in Equation (29b) we find that

$$\int_0^\infty r \, e^{-\frac{r^2}{2\sigma_1^2}} J_0\left(j \frac{rAB}{\sigma_1^2}\right) dr$$

$$= \sigma_1^2 \exp \frac{A^2 B^2}{2\sigma_1^2} = \sigma_1^2 \exp \frac{A^2 D^2 + A^2 S^2}{2\sigma_1^2} \tag{30a}$$

$$\int_0^\infty re^{-\frac{R^2}{2\sigma_1^2}} J_n\left(\frac{jrAB}{\sigma_1^2}\right) dr$$

$$\tag{30b}$$

$$= \frac{\Gamma\left(\frac{n+2}{2}\right)}{\Gamma(n+1)} \left(\frac{jAB}{\sqrt{2}\,\sigma_1}\right)^n \sigma_1^2 M\left(\frac{n+2}{2}, \, n+1; \, \frac{A^2 B^2}{2\sigma_1^2}\right)$$

and the density for ϕ_1 reduces to

$$p(\phi_1) = \frac{1}{2\pi} + \frac{1}{\pi} \exp\left[\frac{-A^2S^2 - A^2D^2}{2\sigma_1^2}\right] \sum_{n=1}^{\infty} \frac{\Gamma\frac{n+2}{2}}{\Gamma(n+1)} \left(\frac{AB}{\sqrt{2}\,\sigma_1}\right)^n$$

$$\cdot\, M\left(\frac{n+2}{2},\ n+1;\ \frac{A^2B^2}{2\sigma_1^2}\right) \cos(n\phi_1 - n\psi). \tag{31}$$

Substitution of Equation (20) for A, Equation (26a) for B, P_{n1} for σ_1^2 and ρ_1 for the sum signal to noise ratio in Equation (31) results in an expression for $p(\phi_1)$ which is a function of ρ_1, ϕ_1, and ψ:

$$p(\phi_1) = \frac{1}{2\pi} + \frac{1}{\pi} \exp\left[-\frac{\rho_1}{2}\left(1 + \frac{D^2}{S^2}\right)\right] \sum_{n=1}^{\infty} \frac{\Gamma\left(\frac{n+2}{2}\right)}{\Gamma(n+1)}$$

$$\tag{32}$$

$$\cdot \left(\frac{\rho_1}{2}\right)^{n/2} \left(1 + \frac{D^2}{S^2}\right)^{n/2} M\left(\frac{n+2}{2},\ n+1;\ \frac{\rho_1}{2}\left(1 + \frac{D^2}{S^2}\right)\right) \cos(n\phi_1 - n\psi)$$

$$\pi > \phi_1 > -\pi$$

The probability density of the random variable $\alpha = -\phi_2$ is derived in the same manner as ϕ_1 and is found to be

$$p(\alpha) = \frac{1}{2\pi} + \frac{1}{\pi} \exp\left[-\frac{\rho_2}{2}\left(1 + \frac{D^2}{S^2}\right)\right]$$

$$\cdot \sum_{n=1}^{\infty} \frac{\Gamma\left(\frac{n+2}{2}\right)}{\Gamma(n+1)} \left(\frac{\rho_2}{2}\right)^{n/2} \left(1 + \frac{D^2}{S^2}\right)^{n/2}$$

$$\cdot\, M\left[\frac{n+2}{2},\ n+1;\ \frac{\rho_2}{2}\left(1 + \frac{D^2}{S^2}\right)\right] \cos(n\alpha - n\psi)$$

$$\tag{33}$$

$$\pi > \alpha > -\pi$$

where ρ_2 is the sum signal to noise ratio in the S−jD channel.

It is assumed that the IF channels are matched in amplitude and phase and have equal noise sources; therefore $\rho_1 = \rho_2 = \rho$.

In order to obtain the density for the difference phase $\phi_1 - \phi_2$ the densities for $p(\phi_1)$ and $p(\alpha)$ must be convolved. Since $\rho_1 = \rho_2 = \rho$, the operation amounts to convolving a function

$$p_1(\phi) = \frac{1}{2\pi} + \frac{1}{\pi} \sum_{n=1}^{\infty} a_n \cos(n\phi - n\psi)$$

$$\pi > \phi > -\pi$$

(34)

with itself. This is a tedious process; however perserverance will yield the result

$$p_2(\Delta\phi) = \frac{2\pi - \Delta\phi}{4\pi^2} + \frac{1}{\pi^2} \sum_n \frac{a_n}{n}$$

$$[\sin(n\pi - n\psi) - \sin(n\Delta\phi - n\pi - n\psi)]$$

$$+ \frac{2\pi - \Delta\phi}{2\pi^2} \sum_n a_n{}^2 \cos(n\Delta\phi - 2n\psi)$$

$$+ \frac{1}{\pi^2} \sum_{\substack{n \\ n \neq m}} \sum_m \frac{a_n a_m}{2} \left[\frac{\sin(n\pi - m\pi - n\psi - m\psi + m\Delta\phi)}{n - m} \right.$$

$$\left. + \frac{\sin(n\pi + m\pi - n\psi + m\psi - m\Delta\phi)}{n + m} \right]$$

$$- \frac{1}{\pi^2} \sum_{\substack{n \\ n \neq m}} \sum_m \frac{a_n a_m}{2} \left[\frac{\sin(m\pi - n\pi - n\psi - m\psi + n\Delta\phi)}{(n - m)} \right.$$

$$\left. + \frac{\sin(-n\pi - m\pi - n\psi + m\psi + n\Delta\phi)}{n + m} \right.$$

$$- \frac{1}{\pi^2} \sum_n \frac{2a_n{}^2}{4n} \sin n\Delta\phi$$

for $2\pi > \Delta\phi > 0$ and

$$p_2(\Delta\phi) = \frac{\Delta\phi + 2\pi}{4\pi^2} + \frac{1}{\pi^2} \sum_n \frac{a_n}{n}$$

$$\left[\sin(n\Delta\phi + n\pi - n\psi) + \sin(n\pi + n\psi)\right]$$

$$+ \frac{2\pi + \Delta\phi}{2\pi^2} \sum_n a_n^2 \cos(n\Delta\phi - 2n\psi)$$

$$+ \frac{1}{\pi^2} \sum_{n\, n\neq m} \sum_m \frac{a_n a_m}{2} \left[\frac{\sin(n\Delta\phi + n\pi - m\pi - n\psi - m\psi)}{n - m}\right.$$

$$+ \left.\frac{\sin(n\Delta\phi + n\pi + m\pi - n\psi + m\psi)}{n + m}\right]$$

$$- \frac{1}{\pi^2} \sum_n \sum_m \frac{a_n a_m}{2} \left[\frac{\sin(-n\pi + m\pi - n\psi - m\psi - m\Delta\phi)}{(n - m)}\right.$$

$$+ \left.\frac{\sin(-n\pi - n\psi - m\pi + m\psi - m\Delta\phi)}{n + m}\right]$$

$$+ \frac{1}{\pi^2} \sum_n \frac{2a_n^2}{4n} \sin n\Delta\phi$$

for $0 > \Delta\phi > -2\pi$.

The next step is to obtain the density for

$$u = f(\Delta\phi)$$

where $f(\Delta\phi)$ is as shown in Figure 3. Now the density for u is related to the density of $\Delta\phi$ through the expressions:

$$p_3(u) = p_2(u) + p_2(u + 2\pi) \qquad 0 \geqslant u \geqslant -\pi$$

$$= p_2(u) + p_2(u - 2\pi) \qquad \pi \geqslant u \geqslant 0 \tag{35}$$

When the indicated opertions are performed, several teams cancel and the density reduces to

$$p_3(u) = \frac{1}{2\pi} + \frac{1}{\pi} \sum_{n=1}^{\infty} a_n^2 \cos(nu - 2n\psi)$$

$$\pi \geqslant u \geqslant -\pi \tag{36}$$

where

$$a_n = \exp\left[-\frac{\rho}{2}\left(1 + \frac{D^2}{S^2}\right)\right] \frac{\Gamma\left(\frac{n+2}{2}\right)}{\Gamma(n+1)} \left(\frac{\rho}{2}\right)^{n/2} \left(1 + \frac{D^2}{S^2}\right)^{n/2}$$

$$\cdot M\left[\frac{n+2}{2}, \; n+1; \; \frac{\rho}{2}\left(1 + \frac{D^2}{S^2}\right)\right] \tag{37}$$

Two limiting cases of Equation (36) are of interest. For ρ vary large the coefficients a_n^2 approach one and

$$p_3(u) \cong \frac{1}{2\pi} + \frac{1}{\pi} \sum_{n=1}^{\infty} \cos(nu - 2n\psi)$$

$$\pi \geqslant u \geqslant -\pi \tag{38}$$

This series is recognized as the Fourier series of a periodic train of delta functions of period 2π centered at $u = 2\psi \pm 2n\pi$. In the restricted interval $\pi \geqslant u \geqslant -\pi$, $p_3(u)$

is a delta function centered at $u = 2\psi$ and the density for the angle measurement is a delta function centered at $\hat{\theta} = \dfrac{\tan^{-1} k\theta_t}{k}$. Thus as $\rho \to \infty$ and $k\theta_t$ small the densities approach the noise free case; the mean of the measurement approaches θ_t and the variance approaches zero as expected. For small values of ρ, the coefficients a_n^2 approach zero and $p_3(u)$ approaches the uniform density:

$$p_3(u) \cong \frac{1}{2\pi} \qquad\qquad \pi > u > -\pi$$

This is exactly the density that would be obtained for the zero signal case. It results in a bias error of $-\theta_t$ and a standard deviation of the error equal to

$$\sigma_\varepsilon = \frac{\pi \, \Delta\theta}{\sqrt{12} \, k_m} \tag{39}$$

These results show that the formulation produces the correct results in the two limiting cases. They also indicate that both the mean and standard deviation of the error are functions of the signal to noise ratio.

Equation (36) can be used in conjunction with Equation (22) to determine the mean and mean square of the angle measurement through the expressions:

$$E(\hat{\theta}) = E\left(\frac{u}{2k}\right) = \frac{1}{2k} \int_{-\pi}^{\pi} u\left[\frac{1}{2\pi} + \frac{1}{\pi} \sum_{n=1}^{\infty} a_n^2 \cos(nu - 2n\psi)\right] du \tag{40a}$$

$$E(\hat{\theta}^2) = E\left(\frac{u^2}{4k^2}\right) = \frac{1}{4k^2} \int_{-\pi}^{\pi} u^2 \left[\frac{1}{2\pi} + \frac{1}{\pi} \sum_{n=1}^{\infty} a_n^2 \cos(nu - 2n\psi) du \right. \tag{40b}$$

When the integrals are evaluated, it is found that

$$E(\hat{\theta}) = \frac{1}{k} \sum_{n=1}^{\infty} \frac{(-1)^{n+1}}{n} a_n^2 \sin 2n\psi \qquad (41a)$$

$$E(\hat{\theta}^2) = \frac{\pi^2}{12k^2} + \frac{1}{k^2} \sum_{n=1}^{\infty} \frac{(-1)^n a_n^2}{n^2} \cos 2n\psi \qquad (41b)$$

These equations indicate that in the general case the mean and mean square of the estimates and hence the mean and standard deviation of the angle error are complicated functions of the signal to noise ratio and the target angle. Detailed evaluation of the mean and standard deviation of the angle error would require families of plots of Equations (41a) and (41b) as a function of signal to noise to ratio for various target angles. Time and funding considerations do not permit such a detailed analysis at the present time.

An interesting special case occurs when the target is on the antenna axis ($\theta_t = 0$). In this instance $\psi = 0$, $E(\hat{\theta}) = 0$ and the standard deviation of the measurement error for a single pulse becomes

$$\sigma_\epsilon = \sqrt{E(\hat{\theta})^2} = \frac{1}{k} \left[\frac{\pi^2}{12} + \sum_{n=1}^{\infty} \frac{(-1)^n a_n^2}{n^2} \right]^{1/2} = \frac{1}{k} g(\rho) \qquad (42)$$

The factor $g(\rho)$ was computed for various values of ρ and the results are tabulated in Table 1. Also listed for comparison purposes are the equivalent factor for the dot product detector, $1/\sqrt{2(\rho+1)}$, and the frequently quoted $1/\sqrt{2\rho}$. Of course the standard deviations of the angle errors are found by dividing the tabulated values by k which is equivalent to multiplication by $\Delta\theta/k_m$ where $\Delta\theta$ is the antenna beamwidth and k_m is the normalized monopulse slope (approximately 1.57 for practical systems.) The data in the table indicate that the S.D. of the error for both the dot product and $S\pm jD$ processors approach $1/\sqrt{2\rho}$ as ρ becomes large ($\rho > 10$). Also the dot product processor errors are smaller than those for the $S\pm jD$

TABLE 1. MONOPULSE ERROR FACTORS

ρ	$g(\rho)$	$\dfrac{1}{\sqrt{2\rho}}$	$\dfrac{1}{\sqrt{2(\rho+1)}}$
0.00	0.90690	∞	0.70710
0.01	0.90470	7.07100	0.70360
0.10	0.88560	2.23600	0.67420
0.25	0.85500	1.41400	0.63250
0.50	0.80730	1.00000	0.57740
1.00	0.72310	0.70710	0.50000
2.00	0.59100	0.50000	0.40820
3.00	0.49500	0.40820	0.35360
4.00	0.42430	0.35360	0.31620
5.00	0.37150	0.31620	0.28870
6.00	0.33140	0.28870	0.26730
7.00	0.30050	0.26730	0.25000
8.00	0.27610	0.25000	0.23570
9.00	0.25660	0.23570	0.22360
10.00	0.24060	0.22360	0.21320
20.00	0.16270	0.15810	0.15430
30.00	0.13150	0.12910	0.12700
40.00	0.11330	0.11180	0.11040
50.00	0.10110	0.10000	0.09901
60.00	0.09208	0.09129	0.09054
70.00	0.08514	0.08452	0.08392
80.00	0.07957	0.07906	0.07857
90.00	0.07496	0.07454	0.07412
100.00	0.07107	0.07071	0.07036

processor for all values of ρ.   One reason for the latter
condition is the idealized model of the AGC, which assumed a
constant output proportional to the square root of the sum of the
signal and noise powers.   The output is a constant only for a
study target RCS and an infinite time constant AGC circuit.   For
finite time constants the AGC output voltage is a random variable
and in practical cases, the dot product results probably conform
more closely to those for the S±jD processor.

1.2   PULSE INTEGRATION

The single pulse measurement errors are modified by the
signal processing and servo systems of the tracker.   Processing
performed prior to the angle measurement is coherent processing
(or integration) since successive pulses are added vectorially
preserving amplitude and phase, coherent processing can be accom-
plished at IF or at baseband if in phase and quadrature
components are preserved.   Noncoherent processing (integration)
refers to signal manipulation after angle measurement and is
associated with the servo in mechanically steered antennas.
Either type of integration can be viewed as forming the average
value of successive samples.

1.2.1   NONCOHERENT INTEGRATION

Noncoherent radars such as magnetron transmitter systems
without phase lock accomplish integration with the servo system
after the monopulse processor.   The servo can be modeled as a low
pass filter with video bandwidth B_S which averages successive
angle measurements over a time interval approximately equal to

$$T_i = \frac{1}{2B_S} \qquad (43)$$

during which

$$N = \frac{T_i}{T} = \frac{1}{2B_s T} = \frac{PRF}{2B_s} \tag{44}$$

measurements occur (T is the radar pulse repetition period and PRF is the pulse repetition frequency). Thus the processed or integrated angle measurement at the servo output can be written as:

$$\hat{\theta} = \frac{1}{N} \sum_{i=i}^{N} E(\hat{\theta}_i) \tag{45}$$

where the θ_i's are the individual pulse measurements.

Since the noise is independent from pulse to pulse, the random variables corresponding to the measurements are independent and the expected value of $\hat{\theta}$ is

$$E(\hat{\theta}) = \frac{1}{N} \sum_{i=1}^{N} E(\hat{\theta}_i) \tag{46}$$

If the signal to noise ratio is constant over the N pulses, then the mean of the integrated measurement is equal to he mean for a single pulse. Thus the servo processing has no effect on the bias error.

Similarly, the variance of the processed estimate is

$$Var(\hat{\theta}) = E(\hat{\theta} - \overline{\hat{\theta}})^2 = E\left[\frac{1}{N} \sum_i (\hat{\theta}_i - \overline{\hat{\theta}}_i)\right]^2 \tag{47}$$

where the bar above a quantity indicates expected value. Independence of the measurements causes Equation (47) to reduce to

$$Var(\hat{\theta}) = \frac{1}{N^2} \sum_i E(\hat{\theta}_i - \overline{\hat{\theta}}_i)^2 \tag{48}$$

For constant signal to noise ratio the variance of the processed error is equal to 1/N times the variance of a single pulse error:

$$Var(\hat{\theta}) = \frac{1}{N} Var(\hat{\theta}_i) \tag{49}$$

Since $\hat{\theta}$ is defined as the sum of the true target angle plus an error ε, the variance of the processed error is also equal to 1/N times the error variance of an individual pulse and the standard deviation of the processed error is $1/\sqrt{N}$ times the standard deviation of the single pulse error. Thus the general expression for the standard deviation of the angle error of a dot product monopulse processor with long time constant AGC and servo integration is

$$\sigma_\varepsilon = \frac{\Delta\theta}{k_m} \sqrt{\frac{B_s}{PRF}} \left[\frac{P_s P_n \left(1 + \left|\frac{D(\theta)}{S(\theta)}\right|^2 + P_n^2\right)}{(P_s + P_n)^2} \right]^{1/2} \tag{50}$$

It should be stressed that while the random error as measured by σ_ε can be improved by the factor $\frac{2B_s}{PRF}$ the bias error is strictly determined by the single pulse value and tracking is seriously impaired for small single pulse signal to noise ratios.

1.2.2. COHERENT INTEGRATION

Coherent integration of successive pulse returns is accomplished by tranmsitter-receiver configurations which process signals of the form

$$s(t) = \sum_n A_o \cos(\omega_o + \omega_d)t \, p(t - nT) \tag{51}$$

where $\sum_n p(t - nT)$ is a periodic video pulse train. The coherent pulse trains are generated by coherent oscillation-power amplifier or power oscillator-phase lock configurations which introduce no relative phase shift on a pusle to pulse basis. Processing can be performed by filtering the entire spectrum of s(t) or a single line thereof. The former type of processing is known as comb filtering or burst waveform processing while the latter is called pulse Doppler processing.

For a range gated pulse Doppler system the peak signal power associated with the filtered central line is

$$S_o = \frac{A_o^2 \, \delta^2}{2T^2} = S_1 \left(\frac{\delta}{T} \right)^2 \qquad (52)$$

where S_1 is the peak power of a single pulse, δ is the pulse length and T is the pulse repetition period. For a doppler filter of bandwidth B_d, the average noise power for the pulse Doppler range gated system is

$$N_o \; (k \, T_o \, B_d \, F) \frac{\delta}{T} = N_1 \left(\frac{\delta}{T} \right)^2 \frac{B_d}{PRF} \qquad (53)$$

where k is Boltzmann's constant, T_o is the reference temperature 290 degrees K, F is the receiver noise figure and N_1 is the output noise power of a receiver matched for a single pulse (bandwidth of $1/\delta$). The signal and noise powers in Equations (52) and (53) are those associated with the input to the monopulse processor. Thus the angle measurement errors $E(\varepsilon)$ and σ_ε have the same form as those derived previously for the dot product and $S \pm jD$ procesors with the single pulse signal to noise ratio

$$\rho_1 = \frac{S_1}{N_1} \qquad (54)$$

replaced by the coherent integration signal to noise ratio

$$\rho_o = \frac{S_o}{N_o} = \rho_1 \frac{PRF}{B_d} \qquad (55)$$

For the dot product processor the mean and standard deviation of the angle error, Equations (12) and (17) become:

$$E(\varepsilon) = \frac{-\theta_t}{1 + \dfrac{\rho_1 \; PRF}{B_d}} \qquad (56)$$

and

$$\sigma_\varepsilon = \frac{\Delta\theta}{k_m} \left[\frac{1 + \left|\frac{D(\theta)}{S(\theta)}\right|^2 + \frac{B_d}{\rho_1 \, PRF}}{2 \, \frac{\rho_1 \, PRF}{B_d} \left(1 + \frac{B_d}{\rho_1 \, PRF}\right)^2} \right]^{1/2} \tag{57}$$

The Doppler bandwidth B_d is determined by the uncertainty in the target Doppler frequency f_d and is much smaller than the radar PRF. Thus

$$\frac{PRF}{B_d} \gg 1.$$

However, the Doppler filter has a response time T_d equal to $1/B_d$ which is usually smaller than the response time of the servo T_i. The equivalent number of independent samples at the Doppler filter output which are noncoherently integrated by the servo is

$$N_i = \frac{T_i}{T_d} = \frac{B_d}{2B_s} \tag{58}$$

Hence the servo procesed angle error for the dot product monopulse has a mean given by Equation (56) and a standard deviation which is reduced by $\sqrt{N_i}$:

$$\sigma_\varepsilon = \frac{\Delta\theta}{k_m} \sqrt{\frac{B_s}{B_d}} \left[\frac{1 + \left|\frac{D(\theta)}{S(\theta)}\right|^2 + \frac{B_d}{\rho_1 \, PRF}}{\frac{\rho_1 \, PRF}{B_d} \left(1 + \frac{B_d}{\rho_1 \, PRF}\right)^2} \right]^{1/2} \tag{59}$$

REFERENCES

1. M. Abramowitz and I.A. Stequn, <u>Handbook of Mathematical Functions</u>, National Bureau of Standards, 1964, p. 486.

Georgia Institute of Technology

ENGINEERING EXPERIMENT STATION

ATLANTA, GEORGIA 30332

27 January 1982

MEMORANDUM:

To: P. P. Britt

From: H. L. Bassett

Subject: "Quick-Look" Radome Analysis

Two radome configurations were analyzed to determine electrical para-
meters at 17 GHz. The first case was that of a slip-cast fused silica
radome with the following dimensions:

Thickness	0.217	inch
Length	20.98	inches
Base Diameter	6.46	inches

In Table 1 are listed the results.. Elevation boresight error (BSEEL),
azimuth boresight error (BSEAZ), elevation boresight error slope (SLPEL),
azimuth boresight error slope (SLPAZ), and transmission loss (GAIN),
are tabulated as functions of seeker antenna look angles (PHI and THETA).
These data in Table 1 are to be used as a baseline design for compari-
sons with the following Case 2 results. The transmission loss for the
slip-cast fused silica radome is plotted in Figure 1.

The Case 2 radome characteristics are:

Length	20.98 inches
Base Diameter	6.46 inches
Outer Skin Thickness	0.030 inch
Core Thickness	0.200 inch

The radome is a two-layer structure with Duroid material for the
outer skin and polyimide quartz for the core or base structure. A
number of cases were run for this configuration allowing for a smooth
ablation of the Duroid material. Results are plotted in Figures 2
through 9. The transmission loss is plotted as a function of look
angle and Duroid material thickness in Figures 2 and 3.

Examples of boresight errors are plotted in Figures 4 and 5 for the uniformly ablating Duroid layer. The boresight error slopes are plotted in Figures 6 through 9 and, as indicated, are shown as functions of antenna look angle and outer skin thickness.

The implications of these results relate primarily to the seeker design and will have a direct result on missile performance. The angular error (boresight error) is a function of

> Antenna Position
> Antenna Aperture
> Nose Shape
> Frequency
> Polarization and
> Wall Construction.

The boresight error varies nonlinearly with the antenna look angle and this is a problem. The overall interrelation between boresight error and missile performance is a complex, nonlinear functional relationship. Techniques have been formulated using a linearized analysis to approximate the effect of boresight error and boresight error slope (rate of change of error with look angle) on overall missile performance. In modeling a seeker tracker system, one considers the stabilization loop and the path by which body motion is coupled into the guidance information. From the seeker subsystem block diagram of Figure 10, note that the radome error is included. Without the radome error, it is known that the line-of-sight rate can be determined without a term containing the missile body angular rate, θ_m. With the radome, the line-of-sight rate is then perturbed by the missile body angular rate and this, in turn, will add a term containing boresight error slope.

To determine if the data from Figures 6 through 9 are meaningful, the seeker would need to be modeled. The primary factors required in the seeker/missile model would be the noise filter time constant, the autopilot time constant, the missile turning rate time constant, the guidance gain, closing velocity, and the seeker/radome boresight error data. By knowing the constants, miss distance calculations can then be made as a function of boresight error slope.

As an example, assume a Mach 1 missile and a Mach 0.8 target engagement, the miss distances would be predicted as indicated in Figure 11 for a target at a 60000 foot altitude. The data in Figure 11 are based on the measured boresight data of Figure 12 and the linear error slope in Figure 13. The actual miss distance would be approximately 7 feet.

This is an example of the models and predictions that are required in assessing missile performance. The example does indicate that the analysis of radome error slope effects plays an important role in an assessment of a missile engagement.

HLB/jm

Computed Electrical Properties, SCFS Radome

RESULTS OF RADOME ANALYSIS
ROCKWELL DUROID POLYIMIDE RADOME
FINENESS RATIO= 3.25 DIAMETER= 6.46000 IN. LENGTH=20.98209 IN.
FREQUENCY= 17.000 GHZ
RA= 1.00000 IN. RB= 1.00000 IN. ANTENNA D= 8.3539 WAVELENGTHS
IPOL= 1 ICASE= 1 IOPT= 1

LAYER	THICKNESS(IN.)	ER	TAND
1	.21700	3.330	.0010

PHI (DEG)	THETA (DEG)	BSEEL (MRAD)	BSEAZ (MRAD)	SLPEL (DEG/DEG)	SLPAZ (DEG/DEG)	GAIN (DB)
.0	.0	-.00	-.00	.0000	.0000	-1.4
.0	2.0	.03	2.33	.0007	.0669	-1.3
.0	4.0	-.00	3.31	-.0007	.0280	-1.0
.0	6.0	-.00	3.56	-.0000	.0070	-.7
.0	8.0	.02	3.03	.0006	-.0149	-.5
.0	10.0	-.00	1.53	-.0006	-.0432	-.4
.0	12.0	-.00	.35	.0000	-.0537	-.3
.0	14.0	.02	-.41	.0005	-.0219	-.2
.0	16.0	.01	-.93	-.0002	-.0148	-.2
.0	18.0	.01	-1.26	-.0001	-.0094	-.2
.0	20.0	.00	-1.47	-.0001	-.0059	-.1
.0	30.0	-.00	-1.59	-.0000	-.0007	-.1
.0	40.0	-.00	-1.26	-.0000	.0019	-.1
90.0	.0	.00	.00	-.0000	.0019	-1.4
90.0	2.0	-2.52	.02	-.0721	.0004	-1.3
90.0	4.0	-4.11	-.00	-.0457	-.0004	-1.0
90.0	6.0	-5.34	-.00	-.0352	-.0000	-.8
90.0	8.0	-5.73	.00	-.0112	.0000	-.6
90.0	10.0	-5.38	.02	.0099	.0005	-.4
90.0	12.0	-4.84	.01	.0155	-.0003	-.3
90.0	14.0	-4.37	-.00	.0153	-.0002	-.3
90.0	16.0	-3.97	-.00	.0115	-.0000	-.2
90.0	18.0	-3.62	-.00	.0101	-.0000	-.2
90.0	20.0	-3.30	-.00	.0091	-.0000	-.2
90.0	30.0	-2.06	-.00	.0071	.0000	-.1
90.0	40.0	-1.24	-.00	.0047	.0000	-.1

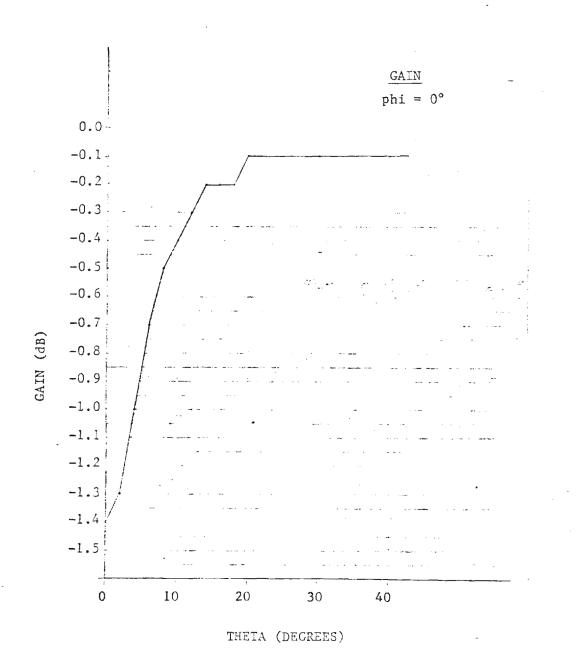RECEIVED SUM VOLTAGE WITHOUT RADOME= .33800E+03

Figure 1a.   Transmission Loss vs Look Angle,
SCFS Radome
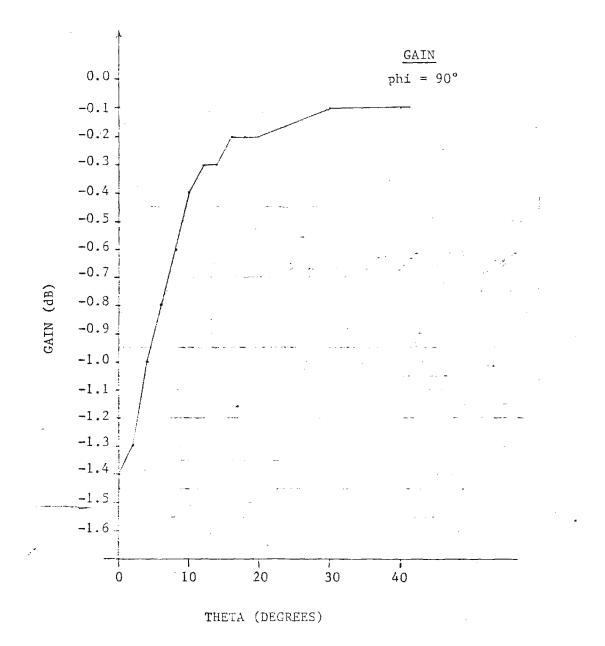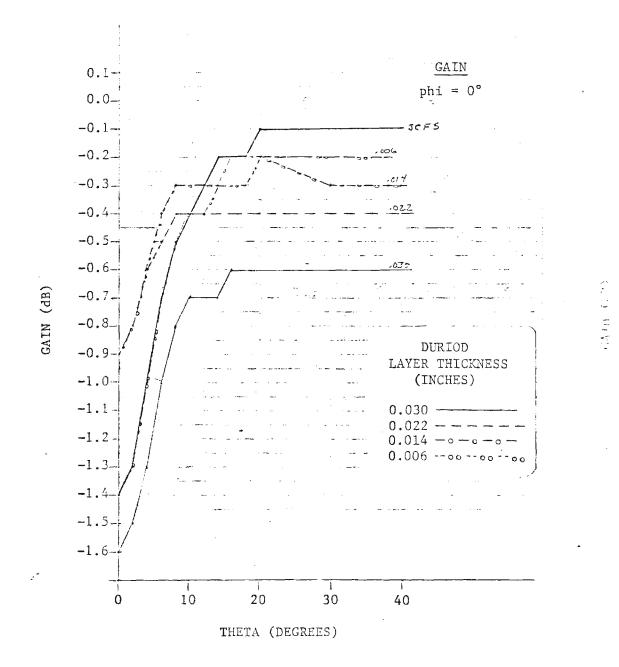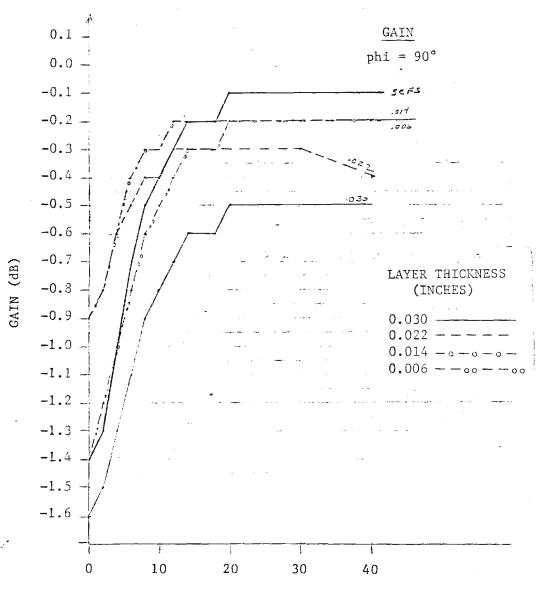
Figure 1b.   Transmission Loss vs Look Angle,
            SCPF Radome

Figure 2. Transmission Loss vs Look Angle,
Duroid Polyimide Radome.

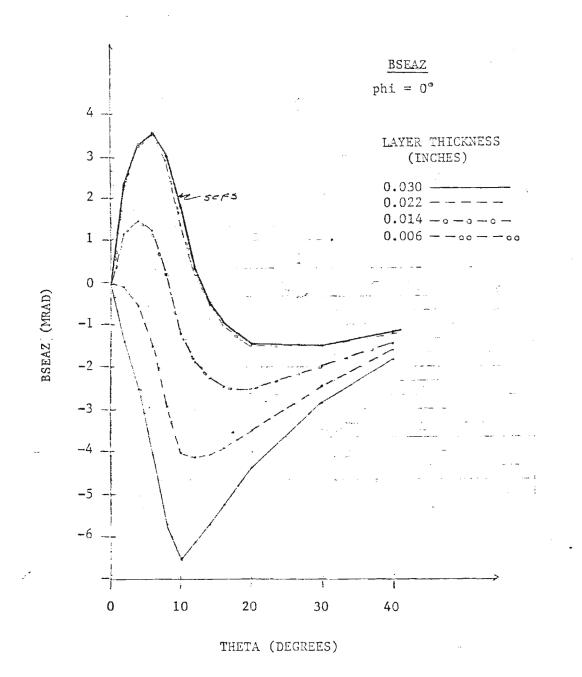Figure 3.   Transmission Loss vs Look Angle,
Duroid Polyimide Radome.

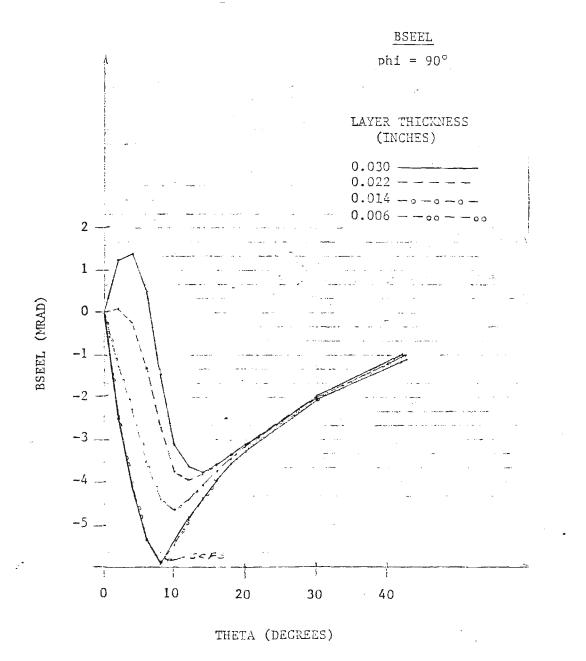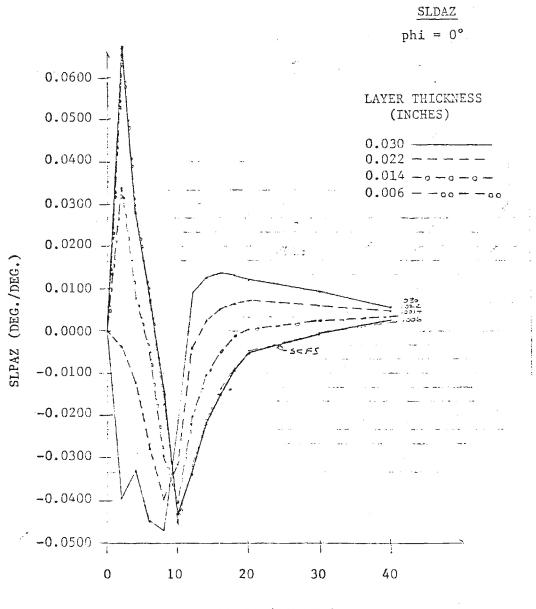Figure 4.   Boresight Error vs Look Angle,
Duroid Polyimide Radome.

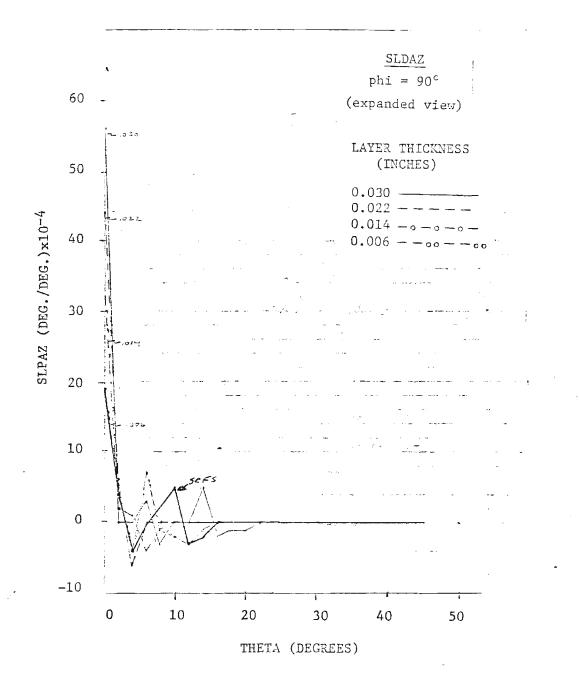Figure 5. Boresight Error vs Look Angle,
Duroid Polyimide Radome.

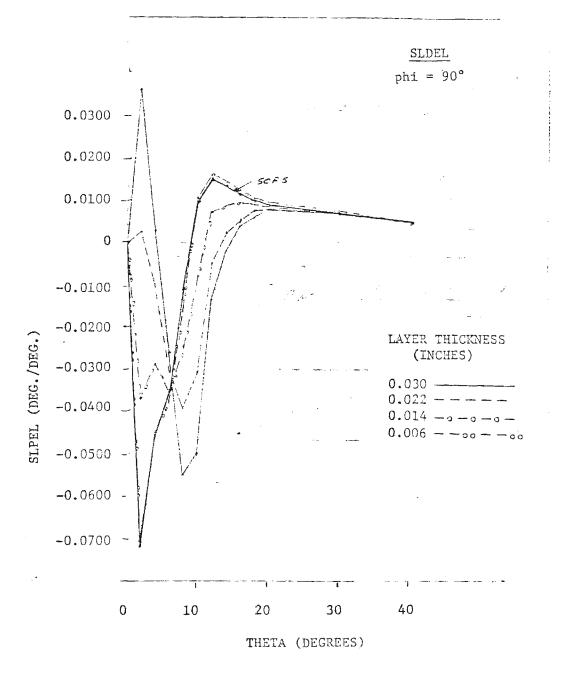Figure 6. Boresight Error Slope vs Look Angle, Duroid Polyimide Radome.

SLDAZ
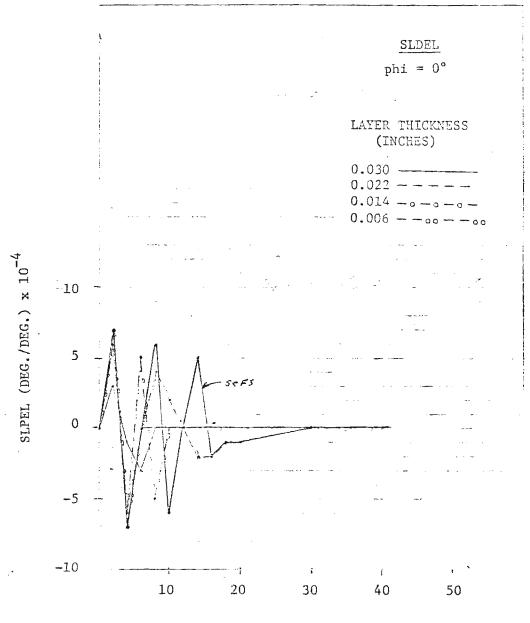
phi = 90°

(expanded view)

LAYER THICKNESS
(INCHES)

0.030 —————
0.022 — — — — —
0.014 —o —o —o —
0.006 — —oo — —oo

Figure 7. Boresight Error Slope vs. Look Angle,
Duroid Polyimide Radome.

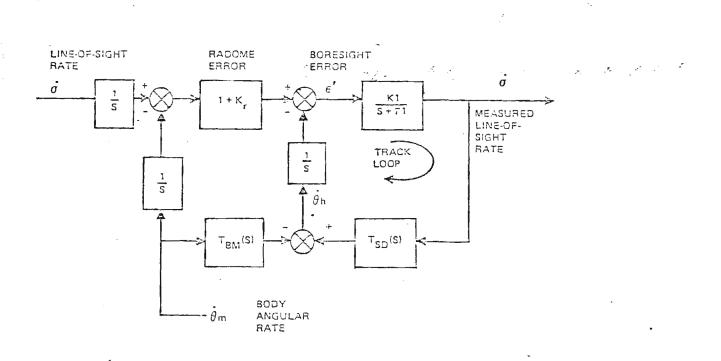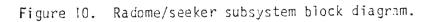Figure 8.   Boresight Error Slope vs. Look Angle,
Duroid Polyimide Radome.

Figure 9. Boresight Error Slope vs. Look Angle,
Duroid Polyimide Radome.

Figure 10. Radome/seeker subsystem block diagram.
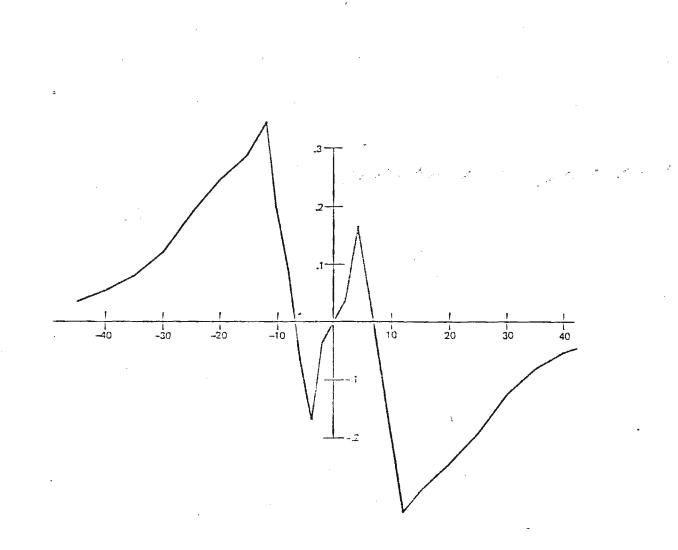
Figure 11. Radome error vs. look angle.
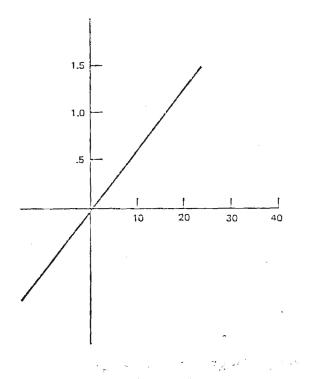
Figure 12.   Error of Figure 11.
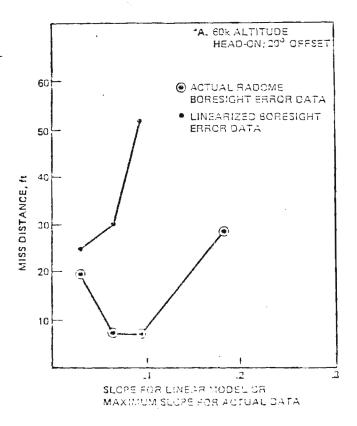   Slope = 0.0625.

Figure 13.   Miss distance as a function of
             radome error slope.

16 November 1981

MEMO

To: Pete Britt

From: Frank Williamson

Subject: Dynetics Report[1] on Meteorological Conditions at
         Minuteman Sites

        The Dynetics report on Meteorological Conditions at Minuteman Sites is a
very ingenous treatment of recorded weather data to obtain a statistical
estimation of the propagation conditions at these sites. Unfortunately, the
recorded weather data was limited in resolution (for instance, rain was
reported as light, moderate, and heavy) and some of the desirable upper
atmosphere data was not available (i.e., cloud top height). Systematic
estimations of the actual weather conditions has been made from the recorded
weather data for this analysis. This estimation process was established with
guidance obtained in referenced literature.

        This report gives radar propagation losses at 35 and 94 gigahertz for
five sensor altitudes. The results of this data analysis is summarized by
seasons for all of the minumteman sites in Figure 3-1. Data from these sites
for all seasons is summarized in the left graph of Figure 1-13. The
attenuation data in these vertical attenuation studies is in absolute units
and is plotted against the cumulative probability that the attenuation will
equal or exceed the value of the graph. Similar cumulative probability curves
for cloud obscuration of the minuteman sites (versus altitude) is given in
Figure 1-12.

        A separate treatment of the weather data has been compiled for the Nevada
area to support the proposed deployment of the MX missile in the multiple aim
point scenario. Since the minuteman site data was presented separately from
the Nevada data, the recent change in the deployment scenario of the MX system
will not effect the usefulness of the data in this report.

        The data in this report appears to be applicable to sensors in anti-ICBM
missiles that are intended for deployment at or near existing minuteman
installations. The vertical attenuation curves may be extended to apply to
slant paths by dividing the attenuation values by the cosine of the zenith
angle.

---

[1] Technical Report, "The Effects of Meteorological Conditions on BMD Sensor
    Performance for Minutemen and MX Deployment Areas," Dynetics, Inc., June 1980.
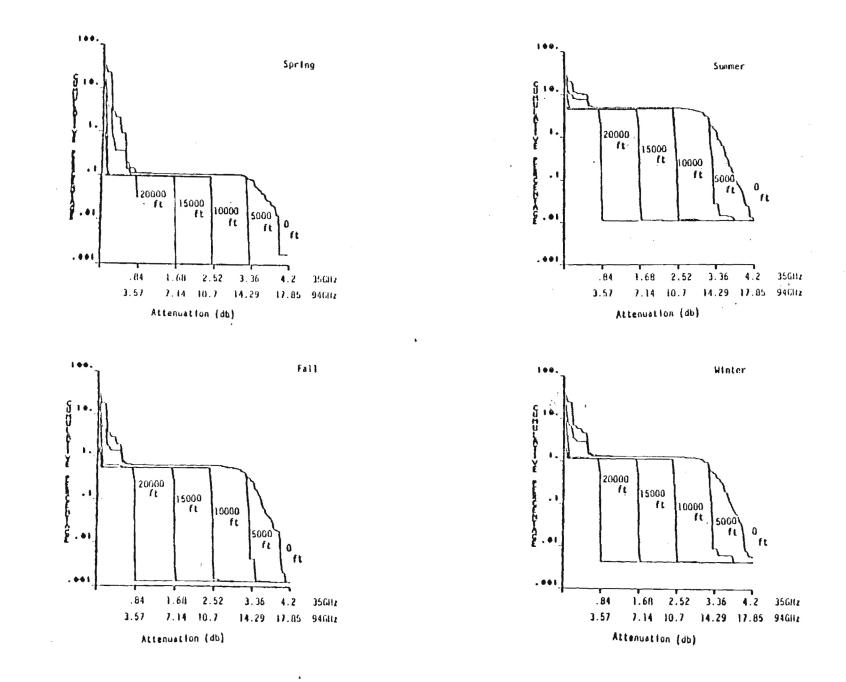
Spring

100.

10.

1.

.1

.01

.001

20000 ft   15000 ft   10000 ft   5000 ft   0 ft

.84   1.68   2.52   3.36   4.2   35GHz
3.57   7.14   10.7   14.29   17.85   94GHz

Attenuation (db)

Summer

100.

10.

1.

.1

.01

.001

20000 ft   15000 ft   10000 ft   5000 ft   0 ft

.84   1.68   2.52   3.36   4.2   35GHz
3.57   7.14   10.7   14.29   17.85   94GHz

Attenuation (db)

Fall

100.

10.

1.

.1

.01

.001

20000 ft   15000 ft   10000 ft   5000 ft   0 ft

.84   1.68   2.52   3.36   4.2   35GHz
3.57   7.14   10.7   14.29   17.85   94GHz

Attenuation (db)

Winter

100.

10.

1.

.1

.01

.001

20000 ft   15000 ft   10000 ft   5000 ft   0 ft

.84   1.68   2.52   3.36   4.2   35GHz
3.57   7.14   10.7   14.29   17.85   94GHz

Attenuation (db)

Figure 3-1.   RF Cloud Attenuation, IMI, by Season

Figure 1-13.   RF Attenuation Due to Clouds

MINUTEMAN SITES -- ALL SEASONS
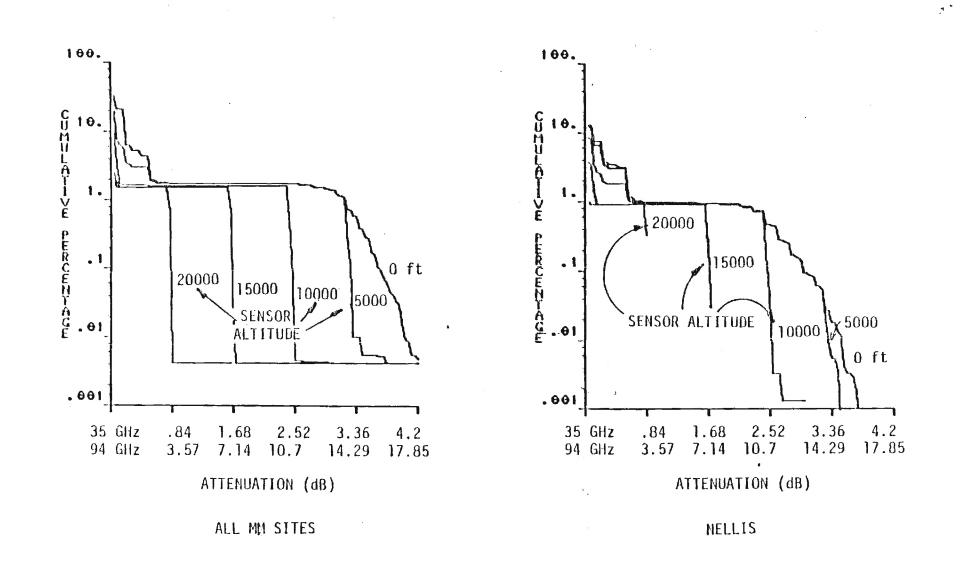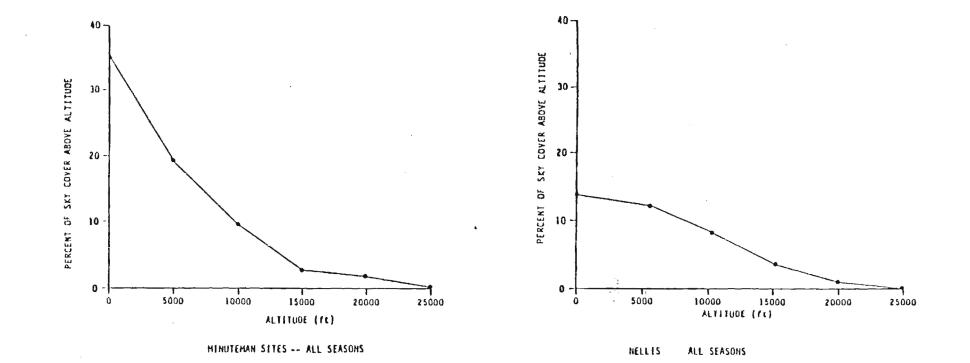
NELLIS   ALL SEASONS

Figure 1-12.   Visible and Near Infrared Obscuration
                Due to Clouds